



Nanostructured proton-exchange membranes from self-cross-linking perfluoroalkyl-free block-co-polymers

Sebastian Auffarth^{a,b,*}, Maximilian Maier^{a,b}, Philipp Martschin^{a,b}, Theresa Stigler^{a,b}, Maximilian Wagner^a, Thomas Böhm^a, Andreas Hutzler^a, Simon Thiele^{a,b}, Jochen Kerres^{a,c,*}

^a Forschungszentrum Jülich GmbH, Helmholtz Institute Erlangen-Nürnberg for Renewable Energy (IET-2), Cauerstraße 1, 91058, Erlangen, Germany

^b Department of Chemical and Biological Engineering, Friedrich-Alexander-Universität Erlangen-Nürnberg, Egerlandstraße 3, 91058, Erlangen, Germany

^c Chemical Resource Beneficiation, Faculty of Natural Sciences, North-West University, Potchefstroom, 2520, South Africa

ARTICLE INFO

Keywords:

Self-assembly
Nanophase separation
Tetrafluorostyrene sulfonic acid
Thiol cross-linking
PFAS-free
Proton-exchange membrane

ABSTRACT

A sustainable hydrogen economy relies on fuel cells and electrolyzers, which heavily depend on ion-conducting perfluoroalkylated materials such as Nafion or Aquivion. Together with other perfluorinated alkyl substances, their environmental accumulation, and the rising awareness of risks to human health stress the need for alternative materials. Based on block-co-polymers from octylstyrene and pentafluorostyrene, we present nanostructured proton-exchange membranes. In contrast to problematic perfluorinated alkyl constituents, the involved aromatic fluorine atoms allow mild functionalizations to form tetrafluorostyrene sulfonic acid. Meanwhile, the nonpolar block reduces the stiffness of the material. By introducing a new preparation technique, controlled mitigation of the thiol cross-linking allows membrane self-reinforcement during drying. The reinforcing cross-links enhance the dissolution stability and reduce the water uptake after 24 h down to 33 wt% at 85 °C. Cross-section imaging visualizes the influence of varying di- and tetrablock-co-polymer backbones on the membrane nanostructure with sizes between 20 and 35 nm. The membranes feature proton conductivities comparable to commercial materials at low humidity levels, surpassing commercial Nafion XL at 87 % relative humidity with up to 79 mS cm⁻¹ at 105 °C. As first successful H₂/air fuel cell tests achieve maximum power densities of up to 0.7 W cm⁻², the nanostructured polymer membranes are a promising candidate for future fuel cell and electrolyzer applications without problematic perfluorinated alkyl substances.

1. Introduction

Per- and polyfluorinated alkyl substances (PFAS) are often labeled "forever chemicals" due to their high chemical stability and environmental persistency [1]. This substance class contains compounds incorporating one or multiple fully fluorinated methyl (-CF₃) or methylene (-CF₂) carbon atoms [2]. In recent years, the accumulation of PFAS in the environment, food chain and humans has been reported more regularly [3–5]. PFAS are related to severe health hazards, leading to a potential restriction by the European Chemicals Agency [6–10]. Members of this material class are highly relevant for electrochemical energy converters. For example, perfluorosulfonic acid polymers are widely used as proton and cation exchange polymers.

Perfluorosulfonic acid polymers like Nafion and its derivatives emerged as standard (membrane) materials for electrochemical

applications [11–13]. Their production is based on the copolymerization of tetrafluoroethylene and sulfonyl fluoride perfluorovinylether, which is later transformed into the respective acid [14]. The excellent proton-conductivity of Nafion relates to the high acidity of the perfluorosulfonic acid group with a pK_a value of around –5.5 [14]. The fluorinated linker to the polytetrafluoroethylene (PTFE) backbone stabilizes the negative charge and enables the formation of aqueous, ion-conducting channels [15]. Despite featuring a mechanically stable backbone and a thermal stability of up to 280 °C, Nafion often limits the application temperature to below 100 °C [16,17]. At higher temperatures, Nafion softens and loses absorbed water, which evaporates above 100 °C at ambient pressure [18,19]. A loss in hydration results in a collapse of the ion-conductive channels to spherical clusters, which leads to a significant drop in conductivity [15,20]. While Nafion is the material of choice for humid, low-temperature hydrogen fuel cells,

* Corresponding authors. Forschungszentrum Jülich GmbH, Helmholtz Institute Erlangen-Nürnberg for Renewable Energy (IET-2), Cauerstraße 1, 91058, Erlangen, Germany.

E-mail addresses: s.auffarth@fz-juelich.de (S. Auffarth), j.kerres@fz-juelich.de (J. Kerres).

<https://doi.org/10.1016/j.mtadv.2024.100521>

Received 29 May 2024; Received in revised form 24 July 2024; Accepted 25 July 2024

Available online 7 August 2024

2590-0498/© 2024 The Author(s). Published by Elsevier Ltd. This is an open access article under the CC BY license (<http://creativecommons.org/licenses/by/4.0/>).

dissolution and fuel crossover challenge the application in liquid isopropanol and methanol fuel cells [13]. Recent reports also confirm the PFAS-related, direct toxicity of the *Nafion by-product 2*, resembling a potential degradation product of Nafion, in animal testing [14,21,22].

For a green energy transition, PFAS-free ion-conductive polymers (ionomers) are required as crucial components in fuel cells and electrolyzers. Materials based on sulfonated polymers with various aliphatic and aromatic backbones have been investigated extensively [23–25]. Often, backbones like polysulfones, polyetheretherketones or polyphenylsulfones are functionalized using a sulfonation reagent and subsequently manufactured as membranes [26–30]. Similarly, highly sulfonated polystyrenes offer high availability and low cost but are brittle if dried and tend to swell drastically in contact with water. Utilizing nonpolar co-polymers adds sufficient mechanical stability to membranes relying on sulfonated polystyrenes [31–33]. For example, a block-co-polymer membrane consisting of partly sulfonated polystyrene and polyisobutylene showed a tenfold increase in conductivity compared to a homopolymer membrane of partly sulfonated styrene [33]. Having a similar ion-exchange capacity (IEC), the block-co-polymer membrane featured continuous nanodomains for enhanced proton transport. Compared to Nafion, the acidity of the sulfonated styrene is reduced to a pK_a value of around -0.56 due to a less charge-stabilizing environment [34].

The presence of electron-withdrawing groups next to an aromatic sulfonic group promotes the stabilization of the negative charge after deprotonation. Therefore, sulfonated poly-*p*-phenylenesulfone (sPSO) or sulfonated polypentafluorostyrene (sPPFS) offer increased acidity (pK_a : $-1.9/-2$), which correlates to an enhanced conductivity of proton-exchange membranes (PEM) [35,36]. The latter ionomer is synthesized from the polymerization of pentafluorostyrene. In contrast to fluorinated alkyl substances like Nafion or other PFAS, polypentafluorostyrene (PPFS) contains only aromatically bonded fluorine atoms. These aromatic fluorine atoms are far more reactive and allow mild substitution with nucleophiles like thiols [37,38]. One major challenge during the functionalization of PPFS is the formation of cross-links after the thiolation [35]. This side-reaction of thiolated PPFS leads to insolubility or highly viscous polymer solutions impeding membrane fabrication. As the final step towards sPPFS, the thiol is oxidized to a sulfonic acid while the rest of the aromatic fluorine atoms increase its acidity. Similar thiolation reactions can completely remove fluorine within polymers based on fluorinated aromatic groups [39–41]. In comparison, the removal of fluorine atoms within PFAS is impossible using these conditions. As PFAS components like tetrafluoroethylene are more industrially established than the polymers from pentafluorostyrene, the latter materials are subject to research and feature higher costs.

sPPFS membranes show promising conductivity, but brittleness and high water uptake remain challenging [35]. Therefore, sPPFS has been grafted onto other polymer backbones for increased mechanical stability [34,42]. Block-co-polymers based on PPFS can feature a nanophase-separated structure due to the self-assembly of polar and nonpolar blocks [43,44]. Block-co-polymers from PPFS and polybutylacrylate were indirectly sulfonated by a mercaptopropane sulfonate, introducing an aliphatic linker that negates the acidity-enhancing effect [44]. A mechanically flexible polyoctylstyrene (POS) block was included in a phosphonated PPFS block-co-polymer. Compared to a pure phosphonated PPFS, brittleness and water uptake were reduced, while concentrating the phosphonated groups into one nanophase increased the conductivity [43].

Based on the controlled synthesis of block-co-polymers from pentafluorostyrene and octylstyrene, this publication utilizes targeted thiol cross-linking to produce self-reinforcing, sulfonated PEMs. Simulations predict the bi-continuous nanostructure of di- and tetrablock polymers, which are validated by scanning transmission electron microscopy (STEM). The block-co-polymer composition controls the formation of lamellar and gyroidal nanostructure with tunable sizes from 20 to 35 nm. The reinforced membranes show reduced water uptake and

brittleness compared to pure sPPFS. Finally, conductivity experiments and first fuel cell tests verify the potential of sulfonated block-co-polymers against PFAS-containing Nafion membranes for future electrochemical applications.

2. Material and Methods

2.1. Nanostructure simulations

All simulations were performed using Materials Studio from BioVia. The characteristics of the homopolymers POS and fully sulfonated sPPFS were calculated by the module Synthia. The mesoscale simulations of the diblock PPFS₅₀-POS₅₀ and the tetrablock PPFS₅₀-POS₅₀-PPFS₅₀-POS₅₀ were carried out using the MesoDyn module. The simulated grid had a spacing of 1 nm and the dimensions 64 nm-64 nm-32 nm. The bond length of 1.1543 nm, the bead diffusion coefficient of $1.0 \cdot 10^{-7} \text{ cm}^2 \text{ s}^{-1}$, the compressibility of 10 kT, and the temperature of 298 K were kept constant for all simulations. While each monomer of the repeating unit was simulated as an individual bead, the number of water molecules per averaged bead was calculated from the molar volumes. Moreover, the interaction energies (see SI-1) were calculated from the van-Krevelen parameters and the molar volumes from Synthia. According to the literature, a van-Krevelen solubility parameter of $25 \text{ MPa}^{0.5}$ was assigned to water [45,49]. The number of steps for each run was set to 200 with a total simulation time of 10 μs . For simulations, the DFT-solver using density and potential space had a tolerance of 0.001 and a maximum amount of 100/300 (without/with water) iterations per step.

2.2. Materials

Commercial 4-*n*-octylstyrene from TCI was destabilized by an alumina oxide column. 4-*n*-Octylstyrene was also synthesized according to a literature procedure [45]. All other chemicals were used without further purification.

2.3. Nuclear magnetic resonance spectroscopy and size-exclusion chromatography

^1H and ^{19}F nuclear magnetic resonance (NMR) spectra were recorded at room temperature on a 500 MHz JEOL JNM-ECZR spectrometer equipped with a ROYALPROBE HFX.

Size exclusion chromatography (SEC) was performed using a *SECurity*² 1260 from PSS. A PSS SDV LUX GUARD was used as a guard column, and three separation columns (2x PSS SDV LUX 3 μm 1000 Å and 1x PSS SDV LUX 3 μm 10000 Å) were applied. The solvent was THF with a flow rate of 1.0 ml min^{-1} at 35 °C. A dual variable wavelength UV-vis (P/N 404–2107, PSS) and a refractive index detector (P/N 404–2106, PSS) were used as detectors. To obtain the relative molecular weight, narrowly distributed polystyrene standards (PSS) were applied for calibration.

NMR and SEC analysis are depicted and analyzed in SI-2 and SI-3.

2.4. Block-co-polymer synthesis

The monomer 1,2,3,4,5-pentafluorostyrene (18.0 g, 12.5 mL, 90.88 mmol, 105 eq), 2-(dodecylthiocarbonothioylthio)-2-methylpropionic acid (DDMAT, 322.0 mg, 0.87 mmol, 1 eq) and azobisisobutyronitrile (AIBN, 29.0 mg, 0.17 mmol, 0.2 eq) were dissolved in tetrahydrofuran (THF, 20 mL). The solution was degassed by three "freeze-pump-thaw" cycles and stirred at 80 °C for 18 h. The monomer conversion was checked by NMR. The yellow reaction mixture was cooled to room temperature and precipitated two times in ethanol. The wet polymer was filtered off and dried at 60 °C overnight to receive a yellow solid (10.6 g, 87 %) which was analyzed by NMR and SEC.

The radical addition-fragmentation transfer (RAFT)-reagent

terminated polymer block (10.0 g, 0.10 mmol, 1 eq) was added to a solution of 4-*n*-octylstyrene (13.1 g, 14.9 mL, 59.93 mmol, 60 eq) and AIBN (33.4 mg, 0.20 mmol, 0.2 eq) in THF (26 mL). The dispersion was degassed by five "freeze-pump-thaw" cycles and stirred at 85 °C for 72 h. The reaction's monomer conversion was screened by NMR and additional AIBN in THF was added two times (20 mg after 20 h, 10 mg after 42 h). The yellow reaction mixture was cooled to room temperature and precipitated in ethanol twice. The wet polymer was filtered off and dried at 60 °C overnight to obtain a yellow solid (15.8 g, 90 %) which was analyzed by NMR and SEC.

The RAFT-reagent terminated diblock-co-polymer (7.0 g, 0.40 mmol, 1 eq) was added to a solution of 1,2,3,4,5-pentafluorostyrene (7.2 g, 5.2 mL, 36.60 mmol, 92 eq) and AIBN (13.3 mg, 0.08 mmol, 0.2 eq) in THF (16 mL). The solution was degassed by three "freeze-pump-thaw" cycles and stirred at 80 °C for 25 h. The reaction's monomer conversion was screened by NMR. The yellow reaction mixture was cooled to room temperature and precipitated in ethanol twice. The wet polymer was filtered off and dried at 60 °C overnight to receive a yellow solid (11.0 g, 96 %) which was analyzed by NMR and SEC.

The RAFT-reagent terminated triblock-co-polymer (9.0 g, 0.31 mmol, 1 eq) was added to a solution of 4-*n*-octylstyrene (5.5 g, 6.3 mL, 25.53 mmol, 80 eq) and AIBN (10.6 mg, 0.06 mmol, 0.2 eq) in THF (16 mL). The dispersion was degassed by five "freeze-pump-thaw" cycles and stirred at 85 °C for 65 h. The reaction's monomer conversion was screened by NMR and additional AIBN in THF was added three times (7 mg after 19 h, 9 mg after 40 h, 5 mg after 46 h). The yellow reaction mixture was cooled to room temperature and precipitated in ethanol twice. The wet polymer was filtered off and dried at 60 °C overnight to obtain a yellow solid (10.2 g, 83 %) which was analyzed by NMR and SEC.

The synthesis of other block-co-polymers was performed accordingly. NMR and SEC analysis are depicted and analyzed in SI-2.

2.5. Functionalization and membrane casting

The diblock-co-polymer (2.5 g, 0.14 mmol_{polymer}, 7.33 mmol_{pentafluorostyrene-units}, 1 eq) was dissolved in argon-purged THF (25 ml), while NaSH-H₂O (3.02 g, 36.6 mmol, 5 eq) was dispersed in argon-purged dimethylacetamide (DMAc, 30 mL) at 55 °C. The polymer solution in THF was added to the stirred DMAc dispersion over 20 min at 55 °C under an argon atmosphere. The color of the reaction mixture changed immediately from turbid yellow to dark turquoise. After the addition of the polymer solution, the conversion was regularly checked by NMR and the reaction mixture was stirred at room temperature. After the targeted substitution degree was obtained within 7 h, the functionalization was terminated by adding water. The reaction mixture changed its color to turbid greenish and was alternately dialyzed (molecular weight cut-off: 6–8 kg mol⁻¹) against water and ethanol over four days. The polymer dispersion was dialyzed against ethanol for 3 h at 55 °C and the yield of thiolated polymer was estimated by drying a fraction of the polymer dispersion (2.9 g, 90 %). N-Methyl-2-pyrrolidone (NMP, 29 mL) was added to the dispersion and excess ethanol was removed under reduced pressure to create a polymer solution (10 wt%). The solution was cast by a doctor blade with a gap height of 800 μm. The film was subsequently dried at 70 °C, 85 °C and 100 °C for around 40 min each and solvent leftovers were removed overnight at 115 °C. Detaching the membrane from the glass plate in water resulted in a 48 μm thick membrane. The membrane was immersed in a mixture of H₂O₂ (30 wt%, 60 mL), formic acid (110 mL) and sulfuric acid (95 wt%, 5.5 mL) for 18 h at room temperature. The oxidation solution was heated to 55 °C for around 2 h to ensure complete oxidation of the thiol groups within the membrane. The membrane was washed multiple times with water until a neutral pH was reached.

Unless noted, the thiolation and membrane production of other block-co-polymers was performed accordingly. NMR analysis is depicted and analyzed in SI-3.

2.6. Raman and infrared spectroscopy

For Raman measurements, a WITec alpha 300 RA confocal Raman microscope (WITec GmbH, Germany) was employed. A 532 nm laser at 15 mW optical power was used for excitation. The signal was collected by a Zeiss W Plan-Apochromat 63x/1.0 objective and a WITec UHTS 300 VIS spectrometer equipped with a 600 grooves/mm optical grating. A home-built sample holder was employed for measuring the samples *in situ* in liquid water at ambient temperature. A Raman spectrum was obtained by averaging three spectra with an acquisition time of 5 s each. WITec Project FIVE+ was used for post-processing by subtracting the signal background with a shape-based algorithm with a noise factor of 1 and a shape size of 400.

Infrared (IR) spectra were recorded using a Spectrum 3 Tri-Range FT-IR Spectrometer from PerkinElmer, Waltham, USA. Membrane samples were directly measured using an attenuated total reflectance unit.

2.7. High-angle annular dark field scanning transmission electron microscopy (HAADF-STEM)

Around 1 cm² of the test membrane was immersed in an aqueous solution of Ba(OAc)₂ (20 wt%) for 4 h at 60 °C. Excess ions were washed away with water multiple times. The membrane samples were embedded in Araldite 502 epoxy resin (Science Services), which was cured overnight at 60 °C. Cross-sections of the samples were prepared by ultramicrotomy on a RMC Boeckeler PowerTome equipped with a Diatome ultra 45 diamond knife. Sections with a thickness of 35 and 60 nm were collected on lacey-carbon-coated grids. HAADF-STEM imaging and STEM energy-dispersive X-ray (EDX) spectroscopy on the cross-sections were performed using a Talos F200i (Thermo Fisher Scientific, Bruker EDS detectors) operated at an acceleration voltage of 80 kV and a beam current around 40 pA. Mean structure size was evaluated by Fourier transformation of the HAADF-STEM-images. The values and errors correspond to the center and the standard deviation of Gaussian peak fitting.

2.8. Ion-exchange capacity

The theoretical IECs of the membranes were calculated from the PPFS-fraction of the block-co-polymers determined by NMR and the thiolation degrees from functionalization. The titrations were performed on an automated titration unit Omnis from Metrohm, Herisau, Switzerland. The test membranes were immersed in supersaturated NaCl solution for 24 h at 85 °C. The solution was titrated against NaOH-solution (0.1 M). The amount of NaOH used to reach the equivalent point was divided by the membrane's dry weight to calculate the experimental IEC_{direct}.

2.9. Water uptake

After determining the dry weight (m_{dry}), the test membranes were immersed in deionized water at 25 °C for 24 h. The wet membrane was removed, and excess water was wiped away. The change in membrane weight ($m_{wet}-m_{dry}$) was divided by the initial weight (m_{dry}) to calculate the water uptake. The procedure was repeated at 60 and 85 °C.

2.10. Dissolution stress test

After determining the initial dry weight ($m_{initial}$), the test membranes were individually immersed in an equi-volumetric mixture of deionized water, isopropanol and acetone at 85 °C for 72 h ($c_{water} = 18.9$ M, $c_{isopropanol} = 4.4$ M, $c_{acetone} = 4.6$ M). The soaked membranes were removed from the solvent mixture and dried at 85 °C overnight. The remaining dry weight ($m_{leftover}$) was divided by the initial dry weight ($m_{initial}$) to calculate the dissolution stability.

2.11. Fenton's test

To investigate the stability of the membrane materials against oxygen radical species, membranes were immersed into an aqueous solution of H_2O_2 (3 wt%) with Fe^{2+} ions (4 ppm, weighed in as $\text{FeSO}_4 \cdot 7\text{H}_2\text{O}$) at 68°C for 4, 10 and 24 h and at 80°C for 1, 2 and 4 h. The remaining test membranes were removed from the mixture, washed with water and dried. The remaining dry weight (m_{leftover}) was divided by the initial dry weight (m_{initial}) to calculate the stability of the membranes. The mixture was dried in a petri dish and redissolved in a sufficient solvent for NMR analysis.

2.12. Stress-strain analysis

The Young's modulus was derived from stress-strain measurements on a DMA 1 from Mettler Toledo, Switzerland, in a tension sample holder, a DMA humidity chamber and a humidity generator MHG32 from proUmid, Germany. The strain was analyzed for a force from 0 to 5 N with an increase of 0.1 N min^{-1} at 25°C and 40 % relative humidity. The stress-strain curve was derived from the force-path diagram and the geometry factor. The Young's modulus and the elongation at break were derived from the stress-strain curve.

2.13. Thermal stability

Thermogravimetry (TGA8000, PerkinElmer) with a heating rate of $10^\circ\text{C min}^{-1}$ and a gas flow rate of 30 mL min^{-1} under a nitrogen

atmosphere was used to analyze the thermal stability of the membrane. The released gases were continuously analyzed by IR spectroscopy (3 FTIR spectrometer, PerkinElmer).

2.14. Conductivity

The conductivities were measured using an MTS 740 from Scribner Associates and the impedance analyzer NumetriQ PSM 1735 from Newton 4th Ltd. The gas diffusion layers H23C2 from Freudenberg were attached to the platinum electrodes of the through-plane holder by the conductive carbon paint Electrodag 502, from Plano GmbH. The test membranes were compressed with around 1.1 psi. The impedance was measured at the given temperatures and humidities over a frequency range of 10 MHz–100 Hz with an AC amplitude of 10 mV with a back-pressure of 1 bar. Due to unknown inductive effects of the measurement setup at very high frequencies (around $>5 \text{ MHz}$), circuit fitting led to unreliable values. Therefore, the membrane resistance was evaluated from the interpolated x-intercept in the Nyquist plot. The specific conductivity was calculated from $\sigma = d \cdot (R \cdot A)^{-1} [\text{mS cm}^{-1}]$ where R is the membrane resistance in, d is the thickness of the tested membrane, and A is the measurement surface. The displayed errors are derived from the mean error of multiple measurements. Strongly divergent measurements due to membrane cracking or contact issues were ignored.

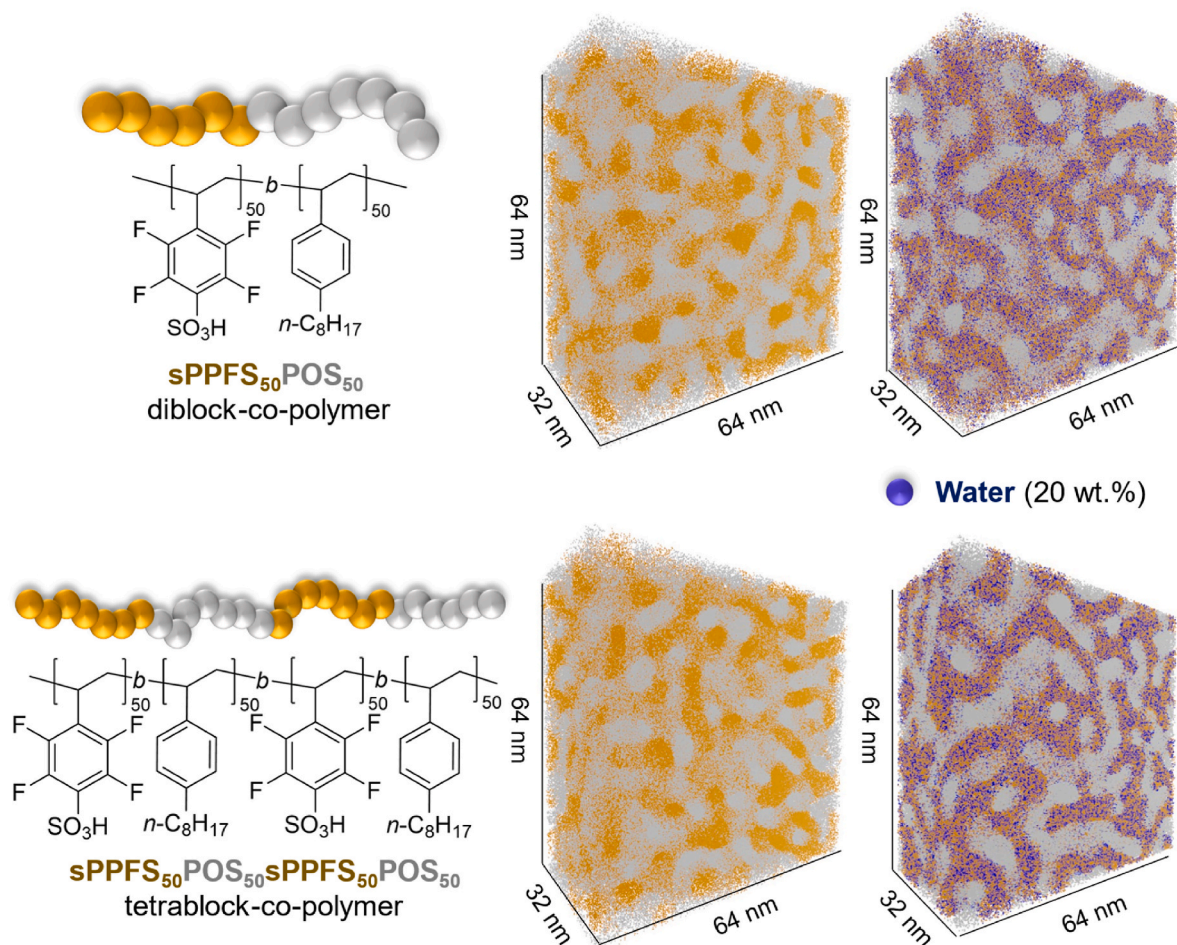


Fig. 1. Nanostructure of di- and tetrablock-co-polymer from sPPFS (orange beads) and POS (grey beads) by mesophase simulations. Simulations on the right side included a water uptake of 20 wt% with multiple water molecules located within each blue bead. (For interpretation of the references to color in this figure legend, the reader is referred to the Web version of this article.)

3. Results and discussion

3.1. Nanostructure prediction

Highly conductive PEMs require strongly acidic groups to generate mobile protons and distinct pathways for proton transport across the membrane. Block-co-polymers tend to perform nanophase separation based on the polarity differences between the blocks and the ratio of their respective lengths [46,47]. To predict the type and size of the nanostructure, mesophase simulations of polymers based on polar sPPFS blocks and nonpolar POS blocks were performed in the software Materials Studios (see Fig. 1). Di- and tetrablock-co-polymers with exactly 50 polar/nonpolar repeating units in each block were used as models. The molar volume and solubility characteristics of both polymer blocks were calculated using the Synthia module, relying on quantitative structure-property relationship methods. With the summarized data in SI-1, the MesoDyn module performed the mesophase simulations of the di- and tetrablock-co-polymers shown in Fig. 1. Here, beads represent each monomer unit in the simulated polymers, distributed across a three-dimensional grid based on their interaction parameters by a component density field. Additionally, the impact of humidity on the simulated nanostructure was investigated by including water beads.

All block-co-polymer simulations show a bi-continuous nanophase with domain diameters around 8 nm consisting of the respective sPPFS and POS blocks. Combining polar nanochannels for proton-transport and nonpolar nanochannels for mechanical flexibility promises ideal characteristics for a PEM. While the nanostructure of the diblock-co-polymer is distributed randomly (MesoDyn order parameter 0.206), the tetrablock-co-polymer exhibits slightly more ordered domains (MesoDyn order parameter 0.221). A tetrablock-co-polymer chain induces a higher order of the nanostructure with less flexibility than two separate diblock chains. Additional water is located within the hydrophilic domains of the simulated block-co-polymers, which increases the polar domain diameter to around 12 nm. The hydrophilic nanochannels filled with water across a PEM are a prerequisite for efficient proton transport in respective applications. Although the uniform chain length of the simulated block-co-polymers cannot be achieved synthetically, a membrane material based on similarly sized POS and sPPFS blocks should offer a bi-continuous nanostructure with hydrophilic nanochannels for proton conduction. Using the same interaction parameters, shorter diblock-co-polymers with 10 and 20 repeating units were also

simulated (see SI-1), but the effect on the domain sizes is negligible. As short polymers entangle less, we decided to synthesize longer polymer blocks to avoid potential problems with poorer film-forming characteristics.

3.2. Polymer synthesis

A controlled polymerization allows the precise synthesis of PPFS-POS block-co-polymers with distinct block lengths influencing the nanostructure of the respective ion-conducting membranes. The addition of a RAFT reagent to the polymerization of the monomer pentafluorostyrene with the radical initiator AIBN yielded a RAFT-terminated PPFS-block, with a narrow dispersity of below 1.1. As depicted in Fig. 2, further blocks of POS and PPFS were sequentially added to generate alternating di- and tetrablock-co-polymers. In contrast to our previous synthesis of POS-PPFS diblock-co-polymers, the work-up and handling of the viscous, RAFT-terminated POS-block was avoided and extended tetrablocks were synthesized [43]. The conversion during each polymerization step was traced by NMR. Table 1 shows the synthesized block-co-polymers and their respective block lengths ranging from 30 to 100 repeating units. The length of each synthesized block was determined by SEC and $^1\text{H-NMR}$ -spectroscopy. The increase of weight-averaged molecular mass in SEC directly correlates to the size of the added block, while the NMR analysis relies on distinct signals from the (macromolecular) RAFT reagent (see SI-2). While the PPFS reached the desired degrees of polymerization within one day, octylstyrene polymerizations often took more than three days and required reinitiation with additional AIBN (see Material and Methods). This observed reluctance may relate to the limited solubility of the nonpolar octylstyrene. The synthesized diblock-co-polymers displayed narrow molecular weight distributions with dispersities of around 1.10–1.20, whereas tetrablock-co-polymers exhibited dispersities of 1.28–1.39. Notably, the molecular weight distributions broaden with each sequential polymerization step (see SI-2) but remain within the typical range of controlled radical polymerizations. The increasing dispersities relate to reoccurring partial chain termination in each step and the need to reinitiate the POS polymerizations. For diblock-1 and tetrablock-1, non-commercial octylstyrene synthesized by a Wittig reaction was used [45]. Related leftovers of phosphoric species may disturb the controlled radical polymerization and could cause the observed 10 % increase in polymer dispersities. Nevertheless, block-co-polymers with different PPFS to POS

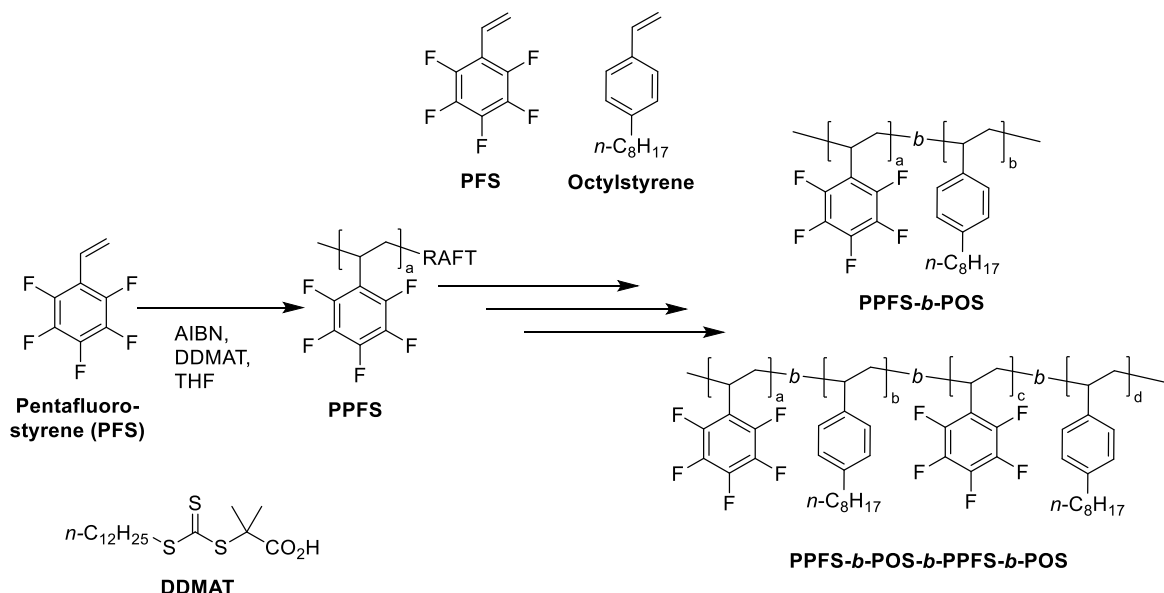


Fig. 2. Stepwise synthesis of PPFS-POS diblock- and tetrablock-co-polymers.

Table 1

Overview of the calculated block sizes (degree of polymerization) from the synthesized block-co-polymers. The given values correspond to the respective analysis method (NMR/SEC). The M_n and M_w were determined by SEC measurements.

Polymer	1. Block: PPFS length	2. Block: POS length	3. Block: PPFS length	4. Block: POS length	$M_{n,SEC}$ [kg.mol ⁻¹]	$M_{w,SEC}$ [kg.mol ⁻¹]	Gravimetric ratio of PPFS: POS
Diblock-1	52/56	35/32 ^{a)}	–	–	14.8	17.7	1.32:1
Diblock-2	82/80	106/98	–	–	33.2	36.6	0.69:1
Tetrablock-1	52/56	35/32 ^{a)}	56/40	40/37 ^{a)}	24.1	33.4	1.28:1
Tetrablock-2	39/38	45/40	50/42	37/26	23.5	29.7	0.97:1

^{a)} POS-block synthesized with 4-*n*-octylstyrene, which was prepared by Wittig synthesis.

length ratios were successfully synthesized.

3.3. Functionalization and cross-linking

As the first step to introduce the sulfonic acid groups (see Fig. 3), the block-co-polymers were thiolated with an excess of sodium hydrosulfide. Thereby, the para-position of PPFS underwent a nucleophilic aromatic substitution. The reaction progress was traced by ¹⁹F-NMR (see SI-3) until the reaction was terminated by the addition of water. Due to the excess of hydrosulfide and a reaction temperature of 55 °C, around 75 % of the *para*-fluoro atoms were substituted within 15 min. As the reaction rate diminished, targeted thiolation degrees between 80 and 90 % were realized by controlling the reaction time (see SI-3). For complete functionalization, external heating had to be reapplied. Conventional polymer precipitation was avoided since subsequent drying

led to the formation of cross-links. This side-reaction inhibits the dissolution of the thiolated polymer, rendering it useless for membrane fabrication.

Salt leftovers and organic solvents were removed by dialysis in water and ethanol. The thiolated polymer formed a turbid dispersion without precipitating. Keeping the thiolated polymer in dispersion minimized cross-linking during the work-up. After NMP was added as a casting solvent, ethanol and water were removed by evaporation. A membrane was prepared from the brown polymer solution by doctor-blading. Subsequently, the dried polymer membranes were oxidized in a mixture of formic acid, sulfuric acid and hydrogen peroxide. Finally, excess acid within the membrane was washed away with water. The membrane denotation includes the synthesized polymer from Table 1 (tetrablocks T1/T2 and diblocks D1/D2) and the achieved thiolation degrees as a suffix.

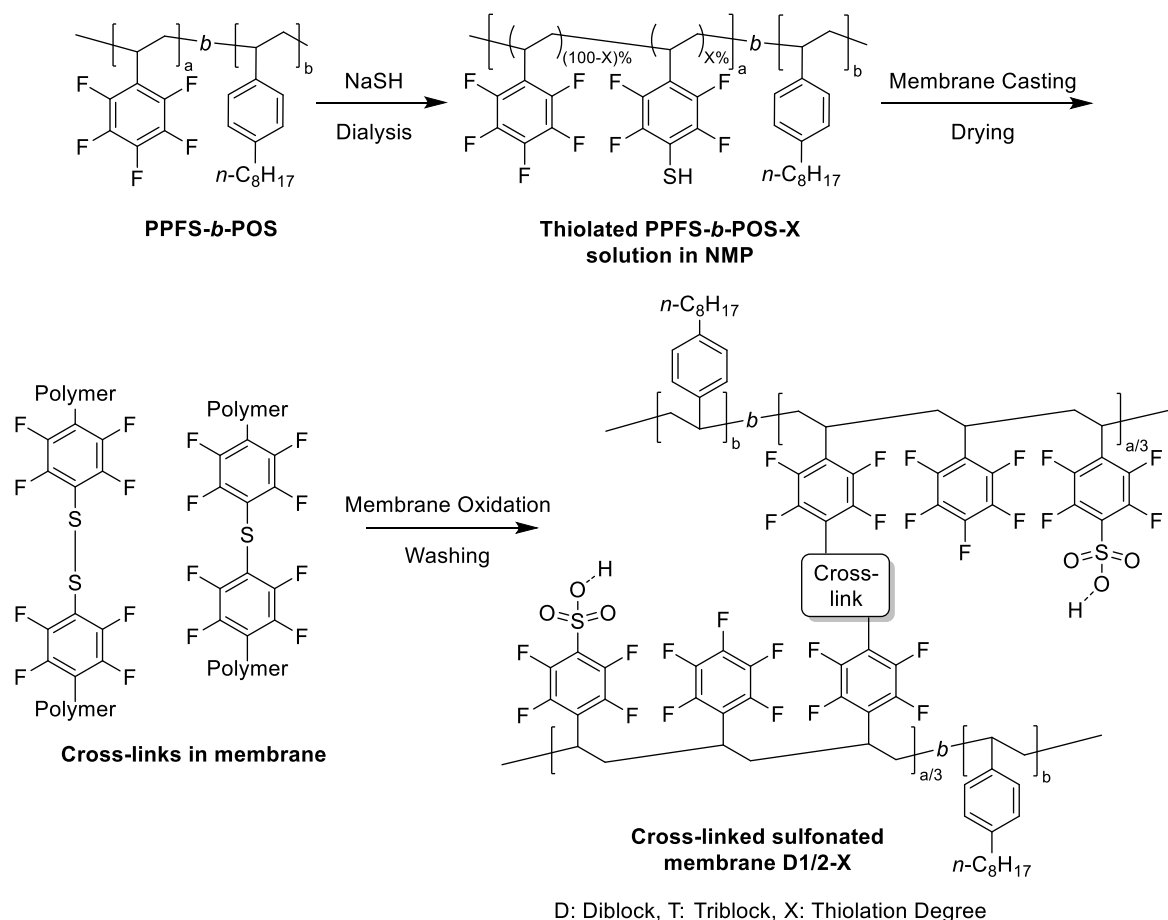


Fig. 3. Overview of the thiolation of PPFS-POS block-co-polymers and subsequent formation of cross-links during solution casting. The oxidation of the thiol groups completes the sulfonation of the membrane. The membrane denotation contains the type of block-co-polymer shown in Table 1 and the thiolation degree from ¹⁹F-NMR-analysis.

After drying, the doctor-bladed polymer solutions formed stable water-detachable membranes. During fast NMP evaporation, merely membrane T1-90 formed cracks, which were prevented by slow pre-drying without external heat for at least five days. This observation highlights the impact of controlled drying on creating a stable membrane, indicating a strong influence of manufacturing conditions on the block-co-polymer system. During the oxidation and washing steps, the membranes based on tetrablocks featured easier handling than their diblock counterparts. The dried block-co-polymer membranes did not redissolve in the casting solvent. This observation relates to the formation of cross-links during the drying process. Raman analysis of the dried thiolated membranes showed characteristic disulfide peaks around 500 cm^{-1} (see Fig. 4-a) [48]. The distinct disulfide peaks remained slightly reduced after the harsh oxidation conditions involving highly concentrated sulfuric acid and hydrogen peroxide. Interestingly, the presence of S-O peaks before the post-treatment (see Fig. 4-a) suggests a partial oxidation with air during the membrane drying step [49]. Further IR analysis (see Fig. 4-b) revealed characteristic SO_3 peaks after post-treatment. Both spectroscopic methods also proved the formation of C-S bonds [49]. Their intensity in IR at 800 cm^{-1} is drastically reduced after the oxidative post-treatment, revealing a minor shoulder. This signal could relate to the proposed C-S-C thioether cross-links.

In our recent findings, the functionalization degree of a related phosphonated diblock polymer had to be limited to around 60 % [43]. Higher phosphonation degrees have led to the disintegration of the membranes into a turbid dispersion when brought in contact with water. Consequently, only membranes with a low number of acidic protons (ion-exchange capacity around 1.2 mmol g^{-1}) were obtained [43]. Here, highly thiolated block-co-polymers (80–100 %) form water-stable membranes by converting a fraction of thiols into cross-links. The spectroscopic analysis and insolubility confirm the successful preparation of cross-linked and sulfonated membranes. Determining the amount of expected and actual number of acidic groups allows an estimation of the ratio of cross-links and sulfonic acids (see section 3.4.2). The presented handling of thiolated PPFS polymers allows mitigation and prevention of side reactions, enabling the practical use of acidic tetrafluorostyrene sulfonic acid as a functional group. As the polymer is in its final form as a membrane, the solubility of the polymer is no longer required. Additionally, the membrane is stable against highly concentrated hydrogen peroxide applied during oxidation. The autonomous formation of cross-links acts as a reinforcement and promises enhanced material properties.

3.4. Membrane characterization

3.4.1. Nanophase imaging

Cross-sections of Ba^{2+} stained membrane samples allow nanostructure analysis by HAADF-STEM measurements. During the staining process, the polar sPPFS-blocks absorb the Ba^{2+} ions, causing an accumulation within the respective domains. The heavy Ba^{2+} ions enhance the mass-thickness contrast of the related nanostructures due to Ruthenford scattering. Therefore, polar sPPFS nanostructures in which the heavy Ba^{2+} ions accumulate appear bright, whereas the nonpolar POS regions remain dark (Fig. 5). Intermediate brightness levels relate to the thickness of the membrane cross-sections (see Material and Methods). Additional EDX-spectroscopy of the nanostructured cross-section in Fig. 5-a depicts the elemental composition of the polar and nonpolar nanophases. While carbon is present throughout both nanophases, heteroatoms like fluorine and barium are only observable in the polar nanophases. These findings confirm the selective staining.

All membrane cross-sections showed distinct nanophase separation forming continuous proton-conducting sPPFS-domains. The repulsive interactions between the polar and nonpolar block-co-polymer compartments drive the formation of these nanophases. According to Table 1, the synthesized polymer backbones can be classified into three groups based on their PPFS to POS ratio. The manufacturing conditions were comparable for all membranes to minimize a potential impact on the nanophase separation in Fig. 5. A PPFS:POS ratio in tetrablock-polymers of around 1:1 (Fig. 5-c, mid) primarily leads to the formation of randomly orientated lamellar nanostructures. The less balanced di- and tetrablocks with PPFS:POS ratios of 0.7:1 and 1.3:1 form (inverse) gyroidal, honeycomb-like nanostructures exclusively. The observed gyroidal nanostructures resemble the results from non-self-reinforcing phosphonated block-co-polymers [43]. The polymer backbone composition realized during synthesis majorly influences the nanostructure of the related sulfonated polymer membranes. Notably, the general nanostructure of the membranes was unaffected by changes in the degrees of functionalization between 79 % and 100 % (see SI-4). Low functionalization degrees were not investigated as the polymers are supposed to be highly proton conductive.

As apparent in Fig. 5-c, the different block ratios affect not only the nanostructure's general shapes but also their sizes. An increased sPPFS amount in the membranes lowers the volume fraction of nonpolar POS in the cross-section images. Thus, the dimensions of nonpolar nanophases shrink. The diffractograms of the HAADF-STEM images were calculated by fast Fourier transformation (see SI-5) to quantify the mean structure sizes (periodicity of the polar nanophase repetition units) [50]. Fig. 5-d shows the decay of average nanostructure sizes from around 34

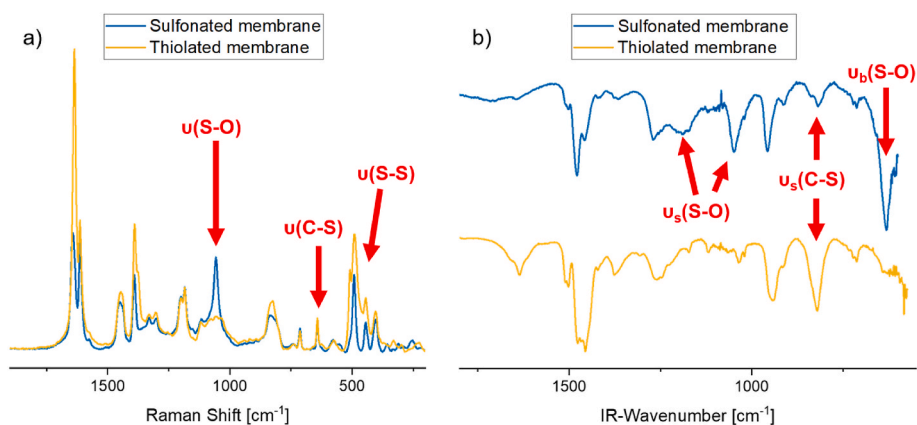


Fig. 4. Raman (a) and IR (b) spectra of the thiolated (yellow) and sulfonated membrane (blue). The Raman spectra are normalized to the signals of the C-H bonds of the backbone around 2900 cm^{-1} . (For interpretation of the references to color in this figure legend, the reader is referred to the Web version of this article.)

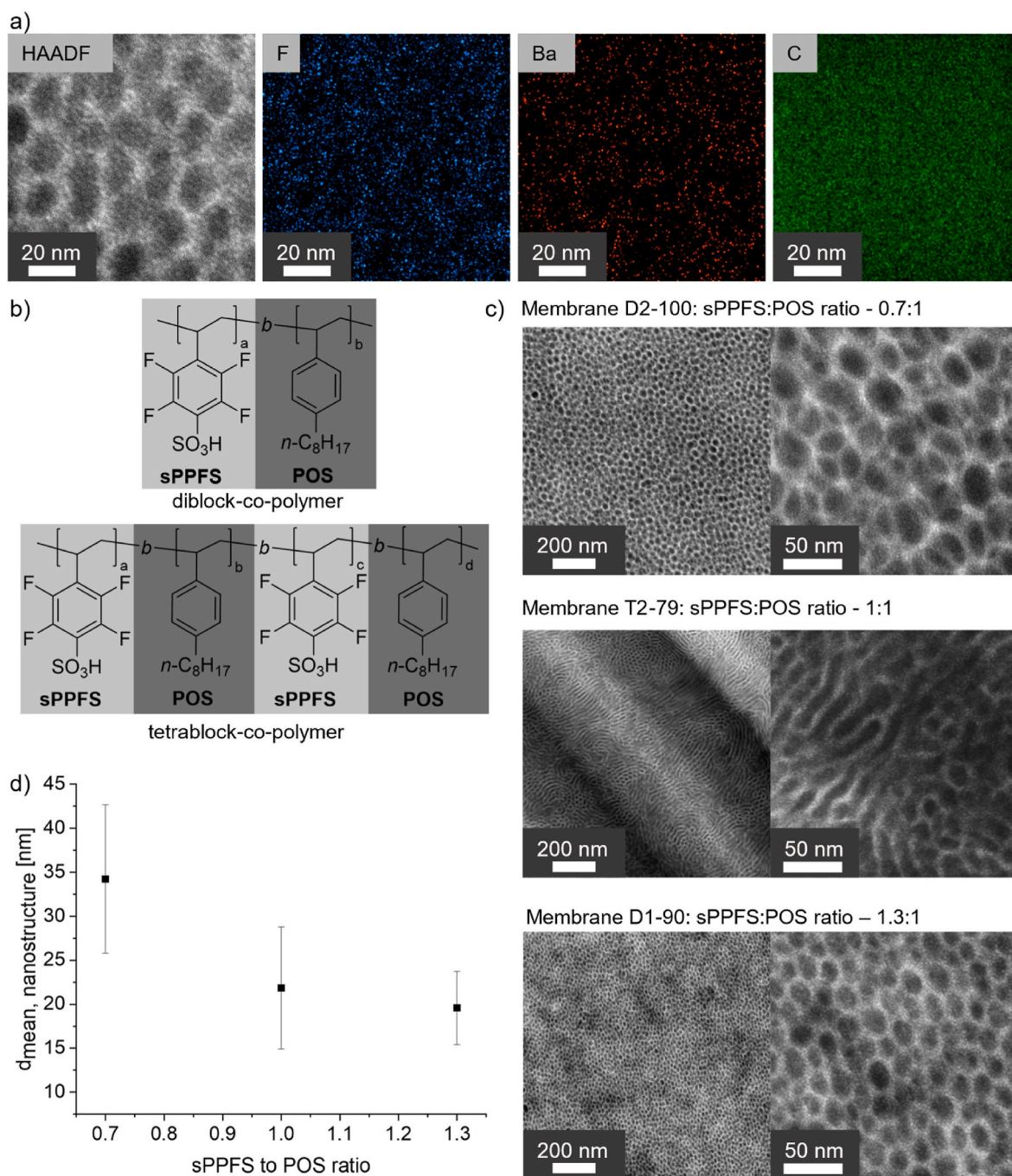


Fig. 5. Nanostructured sulfonated block-co-polymer membranes. (a) HAADF-STEM and EDX spectrum images of a membrane cross-section with enhanced contrast of fluorine and barium for clarity. (b) Simplified chemical structures of the fully sulfonated di- and tetrablock-co-polymer without cross-links. (c) HAADF-STEM images from cross-sections of membranes with increasing sPPFS to POS ratio from top to bottom. (d) Mean structure sizes against the sPPFS to POS polymer ratio.

± 8 nm for membrane D2-100 to 20 ± 4 nm for membrane D1-90, where the sPPFS:POS ratio is roughly doubled. For gyroidal structures, smaller domain sizes decrease the tortuosity for protons transported through the membrane. Straight through-plane transport offers the shortest possible pathways. Reported membranes from the literature featuring lamellas lack the correct alignment of their linear nanostructures, reducing proton conductivity [51]. Similarly, the cross-section of membrane T2-79 with a block ratio of around 1:1 features 22 ± 7 nm wide lamellas without a preferred orientation.

The imaged membrane cross-sections feature a more distinct gyroidal/lamellar nanostructure than predicted by the simulation (Fig. 1). Next to the ideal, uniform polymer lengths, the simulation relied on

simplified, equally sized beads for sPPFS/POS repeating units. Nevertheless, the simulated nanostructure sizes of around 16 nm (diameter of two domains) are within the margin of error of D1-90 and T2-79. The simulations also predicted the general bi-continuous character of the block-co-polymer membranes correctly. The polar domains of the block-co-polymers are larger than for Nafion, which are around 3–5 nm [15]. An earlier analysis of the sPPFS homopolymer revealed a structuring of its polar acid groups and the nonpolar pentafluorostyrene backbone with a diameter of 1.6 nm. Depending on the hydration, the domain spacing of the sPPFS detected by X-ray and neutron imaging increased to up to 3 nm as additional water domains formed [35]. As a fraction of the block-co-polymers consists of pure sPPFS, a similar separation within

the bigger polar nanophases is expected in the presence of water.

The high local concentration of acidic protons and continuity of the sPPFS/POS domains promise enhanced membrane properties. Fortunately, the self-reinforcing cross-link formation does not prevent the formation of related nanophases. The polymers with a PPFS:POS ratio of around 1.3:1 allow higher ion-exchange capacities due to their prolonged functionalizable PPFS compartment. Next to their finer nanostructure, their increased number of proton carriers promises enhanced conductivities. Therefore, the following section further discusses respective di- and tetrablock membranes originating from the same polymer batch.

3.4.2. Ion-exchange capacity, water uptake, stability and mechanical analysis

Fig. 6 compares the experimental and theoretical IECs of the manufactured membranes. The latter values refer to the maximum possible number of ion-exchange groups calculated from the respective block-co-polymer composition and thiolation degree. Therefore, a higher ratio of PPFS to POS in the block-co-polymer and a near maximum thiolation degree result in higher values for IEC_{theo} . IEC_{exp} corresponds to the actual amount of sulfonic acid groups within the membrane calculated by titration and ranges between 1.24 and 1.66 $mmol(H^+) g^{-1}$. A clear discrepancy between IEC_{theo} and IEC_{exp} of around 25–40 % consistently appears for all measurements. A minor part of this discrepancy could relate to uncertainties during the measurements and the NMR-based evaluation of the block-co-polymer sizes. Extensive inclusions of hydrophilic domains, inaccessible by titration, seem unlikely based on the continuous nanostructure revealed in STEM analysis. While the calculation of IEC_{theo} considers every thiol group to be oxidized to the respective sulfonic acid group, in reality, a fraction of the thiol groups is consumed by the formation of cross-links (see section 3.3). A thiol ether reduces the number of achievable acid groups by one, while one disulfide cross-link prevents the formation of two sulfonic acid groups. Therefore, the IEC_{exp} represents the actual amount of retained sulfonic acids within the membrane, while the difference to IEC_{theo} relates to acidic groups lost due to cross-link formation. Nevertheless, the titrated IEC_{exp} seems to correlate with IEC_{theo} and the thiolation degree, as D1/T1-90 and D1/T1-82 differ around 0.3 $mmol(H^+) g^{-1}$. Since Raman spectroscopy only allows a qualitative analysis of cross-link formation,

IEC_{exp} allows a quantitative estimation of the extent of cross-linking. Despite the unclear ratio of disulfide and thioether cross-links, at least 25 % of the thiol groups are involved in the self-reinforcing cross-linking step. Interestingly, membrane T1-90 had the lowest difference between titrated IEC_{exp} and calculated IEC_{theo} . As mentioned in the previous section, T1-90 was dried at ambient conditions for multiple days, which increases the chance of oxidizing the thiol groups with air. Once (partially) oxidized, the functional groups cannot form further cross-links, which increases IEC_{exp} . The oxidation of the dispersed thiolated block-co-polymer before membrane casting might further close the gap between IEC_{theo} and IEC_{exp} .

The mechanical stress induced by water uptake can impact the lifetime of a membrane material in its respective application. Generally, a high IEC of a membrane material induces an increased water uptake due to the higher number of water-attracting ionic groups. The observed water uptake behaves accordingly, as D1-90 has a water uptake of up to 77 wt% at 85 °C, while its low IEC counterpart D1-82 exhibits half the water uptake across all temperatures (see Fig. 7). The tetrablocks T1-90/T1-82 swell less than their diblock equivalents due to their increased chain length and enhanced capability to form cross-linked networks with both hydrophilic blocks. Notably, T1-90 features up to 30 % less water uptake than D1-90 at 25 °C despite having a similar IEC. This difference is less pronounced for the low IEC couple D1/T1-82. Compared to commercial Nafion (composite) membranes, all block-co-polymers take up more water at low temperatures. This observation relates to the larger hydrophilic domains of the block-co-polymer compared to the nanostructure induced by the alkyl spacers in Nafion (15–5 nm vs. 3–5 nm) and the lower IEC of 0.91 $mmol g^{-1}$ [14,15]. Remarkably, the relative change in water uptake by increasing the temperature is lower for the block-co-polymer membranes. Once the domains are loaded with water, the cross-links hold the polar nanophase in place and prevent further water uptake. On the contrary, Nafion does not contain covalent cross-links and shows additional water uptake with increasing temperature. This feature is unique for directional covalent cross-links. In contrast, conventional acid-base blending relies on the interaction between negative and positive charges, which water can disturb at higher temperatures, consequently reducing their effectiveness [52]. In literature, pure sPPFS has shown 3.5 times higher water uptake than Nafion and tends to be water soluble at higher

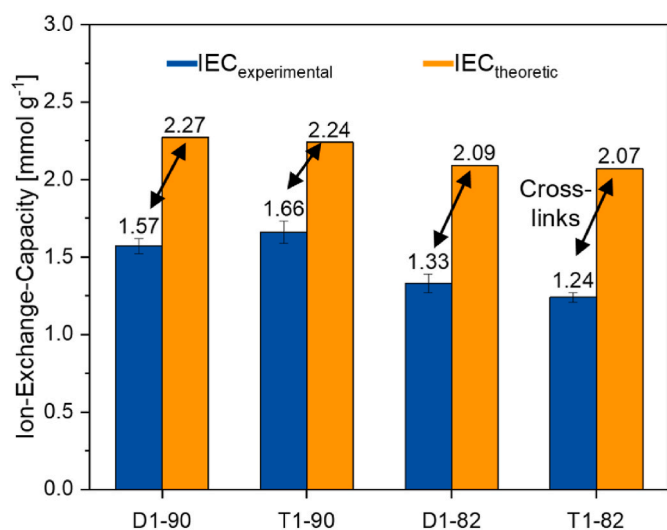


Fig. 6. Comparison of experimental (blue, error bars indicating standard deviations from three measurements) and theoretical (orange) IECs of the sulfonated block-co-polymer membranes. The difference in IEC (marked as black arrows) relates to the formation of stabilizing cross-links during membrane production. (For interpretation of the references to color in this figure legend, the reader is referred to the Web version of this article.)

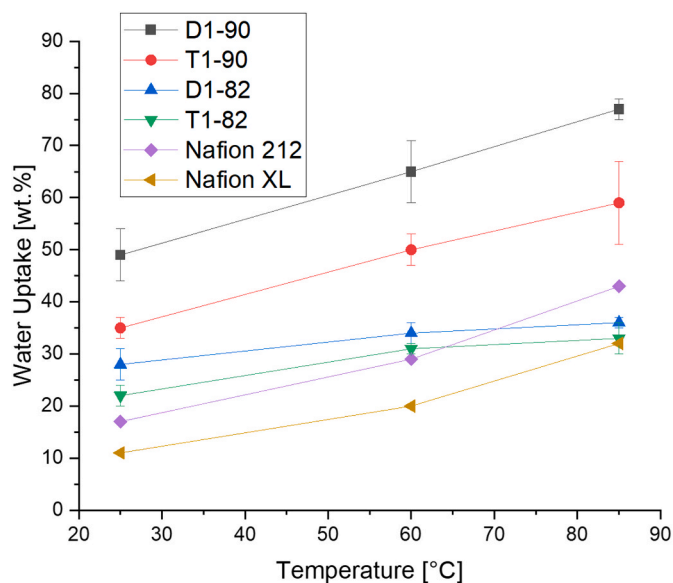


Fig. 7. Water uptake of the sulfonated block-co-polymer membranes and commercial Nafion membranes at given temperatures. Measurements were repeated at least three times to calculate the average value and the standard deviation.

functionalization degrees [35]. Due to the reinforcing covalent cross-links, the detected 33–36 wt% water uptake of D1/T1-82 is between Nafion XL and Nafion 212 at 85 °C. A compromise between water uptake (which improves proton conductivity) and limited membrane swelling (which prevents stability issues in PEM-based systems) is especially relevant for application.

The stability of the block-co-polymer membranes against dissolution was tested to investigate a potential application within direct isopropanol fuel cells. In a stress test within a mixture of water, isopropanol, and acetone (see Material and Methods), the membranes resisted dissolution and showed only a minor mass loss of less than 6 % (see Table 2). However, only D1-82 and T1-82 maintained sufficient mechanical stability after the test. During removal from the test solutions, the swollen membranes D1-90 and T1-90 broke into smaller pieces that needed to be filtered off. While Nafion 212 dissolves during this harsh stress test, the observed stabilities relate to the reinforcing cross-links within the block-co-polymer membranes. During the membrane post-treatment, the cross-linked membranes withstood strong oxidative acidic environments of 10 wt% H₂O₂. To further investigate the stability against radicals, T1-82 was exemplarily characterized in a Fenton's test. After 1 h at 80 °C, the membrane retained its mechanical properties and initial mass. The first degradation was observed after 2 h when 95 wt% of the initial membrane mass was detected. However, after 4 h, only a strongly turbid dispersion was found. NMR analysis of a related dispersion (see SI-6) revealed a stronger degradation of the POS block compared to the sPPFS. The NMR results suggest a faster degradation of the POS-nanophase, which could destabilize the remaining membrane to form a polymer dispersion. The formation of intact sPPFS-rich polymer particles in Fenton's reagent would also relate to the increased turbidity over time. Using an alternative hydrophobic polymer block could further increase the membrane material's stability.

All presented block-co-polymer membranes consist of two types of polymers with drastically different individual thermal and mechanical behaviors. While POS alone displays a very low glass transition temperature (T_g) of -20 °C, the sulfonic acid groups in sPPFS push the respective T_g above 160 °C [35,43]. Therefore, each homopolymer by itself would be a viscous fluid or a brittle solid under standard conditions. By combining these properties, the block-co-polymer membranes exhibited sufficient mechanical stabilities during their characterization in general. To quantify the mechanical properties of the membranes, stress-strain analysis was performed to calculate the Young's moduli and the elongation at break (see Table 2).

Young's modulus describes the elastic deformation of a solid and rises for brittle materials. While the brittle sPPFS has a very high Young's modulus of 569 MPa, the presented membranes display lower Young's moduli and good flexibility due to stiffness-reducing POS. With 240 ± 27 MPa, the tetrablock T1-82 has a higher stiffness than the respective diblock-co-polymer D1-82 with a Young's modulus of 171 ± 7 MPa. This behavior is expected since the two sPPFS blocks participate in two different polar nanophases, resulting in a more robust reinforcing

network through thiol cross-linking. D1-90 and T1-90 should have similar stiffnesses to their low IEC counterparts since all membranes have a cross-linked sPPFS nanophase. However, the measured Young's moduli only validate this expectation for the diblock-based membrane D1-90. In contrast, the Young's modulus of 43 ± 7 MPa measured for T1-90 undercuts all other tested membranes. The discrepancy of T1-90 is likely generated by the different drying methods during membrane manufacturing. The related prior oxidation with air may reduce the amount of self-cross-linking and impact the mechanical behavior. This observation highlights the impact of manufacturing and might enable further improvements of the material properties in future studies. In addition, the elongation at break of the membrane materials was analyzed (see Table 2). The highly brittle homopolymer sPPFS already fails at 2.4 ± 0.7 % elongation, while the block-co-polymers roughly triple the elongation at the point of failure. The POS-nanophase softens the material for low stress but cannot compensate for the brittle cross-linked sPPFS at higher elongation. At similar conditions, commercial Nafion membranes sustain 180–200 % elongation before failure, according to the literature [14,53]. Nevertheless, the block-co-polymers substantially ease the handling compared to the sPPFS homopolymer, which often shattered even before testing.

To investigate the thermal stability of the block-co-polymers, membrane T1-90 was exemplarily characterized by thermal gravimetric analysis (TGA). Fig. 8 displays the temperature-induced degradation and related IR analysis. The weight loss between the temperature range 30–200 °C represents residual water present in the polymer matrix. The second weight loss step with $T_{\text{Onset}} = 263$ °C gives rise to signals in the IR at 2936 cm⁻¹, which can be assigned to -CH₂ and -CH₃ vibrations [49]. The signal at 1373 cm⁻¹ is associated with SO₂-bands, which indicate the decomposition of sulfonic acid groups and is typically seen at a temperature range of 250–300 °C [35,54]. The step from 263 °C to 427 °C exhibits a reduction in weight of around 26 %, corresponding to the loss of octyl chains and sulfonic acid groups. At $T_{\text{Onset}} = 427$ °C signals for valence vibration of -CH₂ units at 2938 cm⁻¹, a sharp signal at 1494 cm⁻¹ from aromatic rings, signals at 1261 cm⁻¹, 1178 cm⁻¹ for C-F vibrations, and a signal at 927 cm⁻¹ attributed to C-H out of plane deformation vibration arise [49]. These signals refer to the styrene repeating units, which indicate the thermal degradation of the polymer backbone. Due to their similar polymer structure, we expect identical thermal behavior from the other membranes. When using synthetic air as a carrier gas, the first polymer decomposition step also occurs around 266 °C (see SI-7). The observed thermal degradation is well above the operation temperature of typical electrochemical applications, confirming the material's stability.

3.4.3. Conductivity and resistance in hydrogen fuel cell test

The through-plane conductivities of the block-co-polymer membranes and commercial Nafion membranes are plotted in Fig. 9. Conductivities were determined between 30 and 105 °C with 50–87 % relative humidity (RH) to mimic a broad range of application conditions for low-temperature fuel cells. At least three samples were prepared and measured for each membrane to calculate an average conductivity and error (see Material and Methods).

At low relative humidities of around 50 %, the conductivity of Nafion 212 is significantly higher than the conductivities of the block-co-polymer membranes. Although Nafion XL contains additives for improved water management, it falls behind Nafion 212 and is similar to the membrane T1-90 with around 13 mS cm⁻¹ (105 °C, 50 % RH). At higher RHs, Nafion XL also lags behind Nafion 212 despite relying on similar perfluorosulfonic acid polymers. The conductivity difference may relate to the PTFE reinforcement within Nafion XL. For 70 % RH, the conductivities are enhanced for all membranes, while the general positioning stays similar. With an average conductivity of 41 mS cm⁻¹ (85 °C, 70 % RH), Nafion 212 is ahead of D1-90/T1-90 and Nafion XL with around 18 mS cm⁻¹, while D1-82 and T1-82 show conductivities of about 10 mS cm⁻¹ at the same conditions. Interestingly, at 30 and 55 °C

Table 2

Dissolution stability and mechanical properties of sulfonated block-co-polymer membranes. Measurements were repeated at least two times to calculate the average value and the standard deviation.

	D1-90	T1-90	D1-82	T1-82	sPPFS	Nafion 212
Dissolution stability in acetone/isopropanol/water mixture [wt.%]	94 ± 1	96 ± 2	95 ± 3	97 ± 1	-	0
Young's modulus [MPa]	150 ± 41	43 ± 2	171 ± 7	240 ± 27	569 ± 3	285 ± 8
Elongation at break [%]	7.4 ± 1.0	6.8 ± 1.1	8.6 ± 2.9	7.1 ± 2.0	2.4 ± 0.7	>180 [14,53]

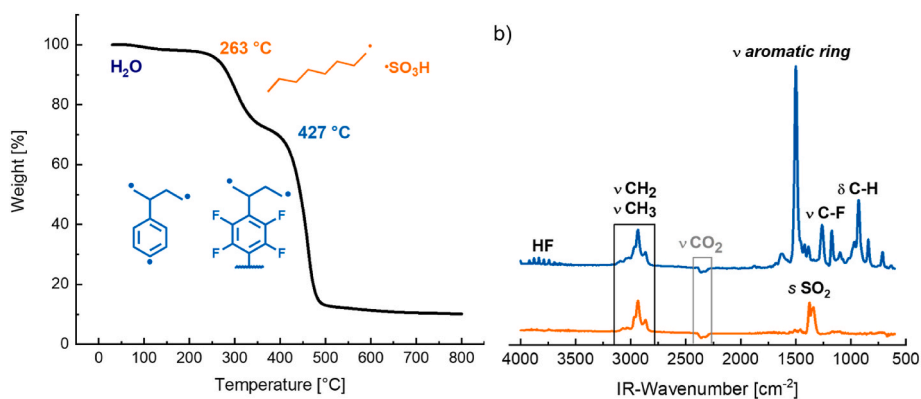


Fig. 8. (a) TGA profile of T1-90 (heating rate: 10 K min⁻¹, carrier gas: nitrogen). (b) IR spectra of gasses released at selected temperatures (orange: T_{Onset} = 263 °C, blue: T_{Onset} = 427 °C). Due to the IR setup, CO₂ in the ambient air is observed. It is not assigned to the decomposition of the polymer. (For interpretation of the references to color in this figure legend, the reader is referred to the Web version of this article.)

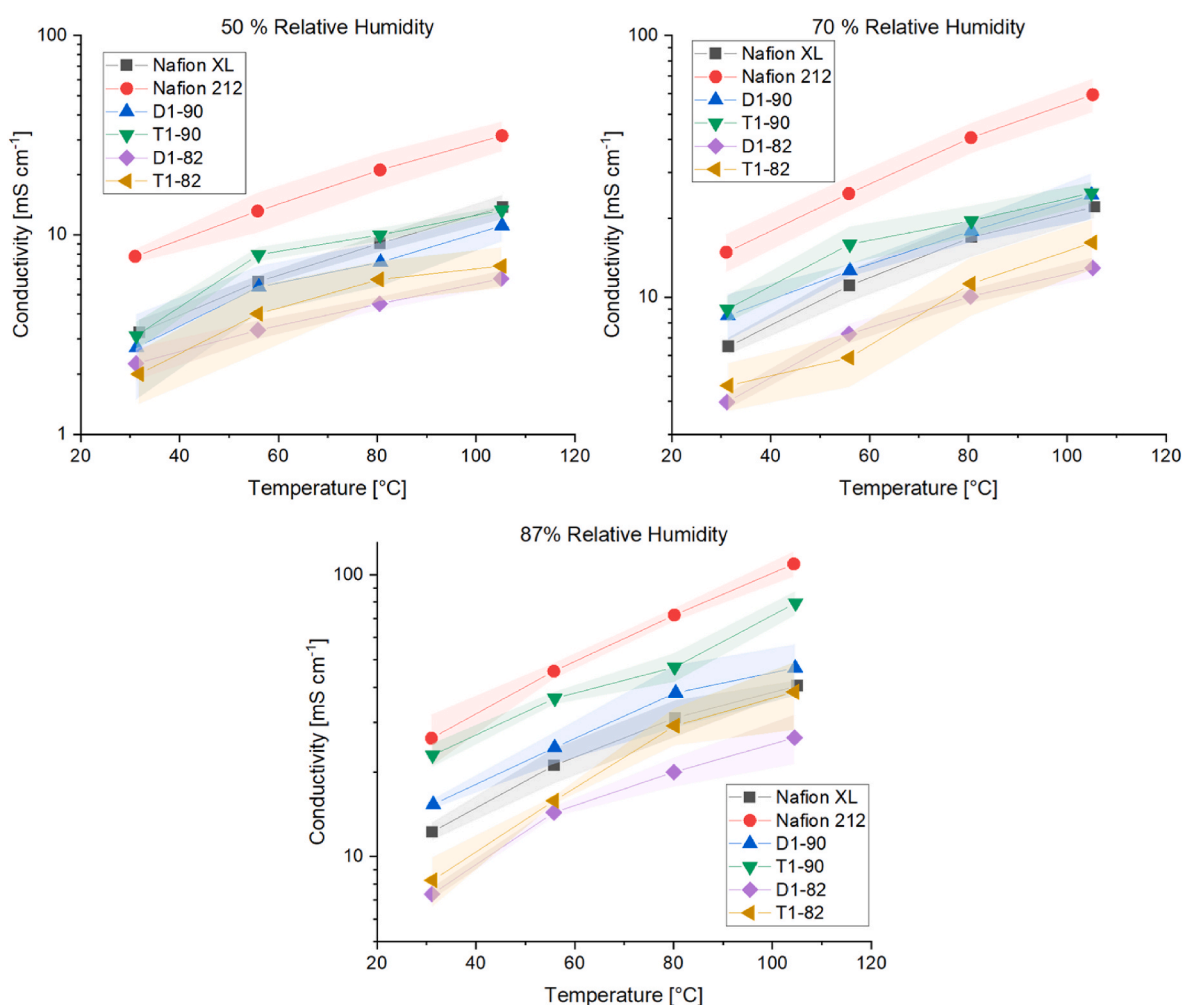


Fig. 9. Through-plane conductivities of commercially available Nafion membranes and block-co-polymer membranes at given humidities against temperatures.

with 70 % RH, T1-90 clearly surpasses the conductivities of Nafion XL. For an increased RH of 87 %, T1-90 features better average conductivities than Nafion XL and the other block-co-polymer membranes for all temperatures with up to 79.5 mS cm⁻¹ (105 °C, 87 % RH). At conditions typical for low-temperature hydrogen fuel cells (80 °C, 87 % RH), T1-90 exhibits an average conductivity of 47 mS cm⁻¹ compared to 34/74 mS cm⁻¹ of PFAS-containing Nafion XL/212. While D1-90 performs similarly to Nafion XL for most temperatures at 87 % RH, the averaged

conductivities of D1-82 and T1-82 slightly fall behind. Nevertheless, the block-co-polymer materials benefit significantly from increased RH; i.e., the conductivity of T1-82 rises from 5 to 30 mS cm⁻¹ (80 °C) by increasing the RH from 50 % to 87 %. In contrast, commercial Nafion membranes only triple their conductivity due to the same RH increase.

Some measurements have a considerable error margin, which likely relates to uncertainties from mounting several samples and the instrument itself (see Material and Methods). Nevertheless, the measurements

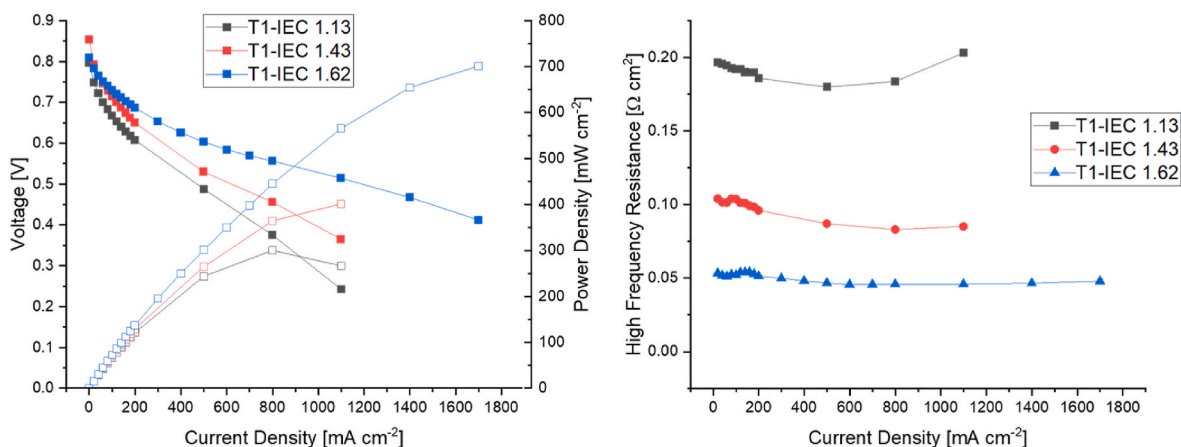


Fig. 10. Membrane-electrode assembly from block-co-polymer membranes with given IEC and Nafion electrodes ($0.3 \text{ mg}_{\text{Pt}} \text{ cm}^{-1}$) in a hydrogen fuel cell test (80°C , 95 % RH).

Table 3

Thicknesses of tested membranes and their HFR in H_2/air fuel cell test. Nafion references are acquired from the given literature.

	Membrane Thickness [μm]	Average HFR [Ohm cm^2]
T1-IEC 1.13	37	0.190
T1-IEC 1.43	32	0.091
T1-IEC 1.62	27	0.049
Nafion XL [55]	28	0.071
Nafion 211 [56]	25	0.056
Nafion 212 [57,58]	50	0.083

follow general trends: Due to the lowest amount of proton-exchange groups, D1-82 and T1-82 (IEC: $1.33/1.24 \text{ mmol}(\text{H}^+) \text{ g}^{-1}$) fall behind the other block-co-polymers in terms of conductivity at various temperatures and humidities. Similarly, T1-90 surpassed the other membranes and even Nafion XL due to the highest IEC of $1.66 \text{ mmol}(\text{H}^+) \text{ g}^{-1}$. The membranes' conductivities, particularly those of the block-co-polymers, benefit from higher humidities due to more water assisting the proton transport. Due to larger hydrophilic domains in the block-co-polymer membranes than in Nafion membranes, more water is required to form continuous proton-conducting water channels throughout the membrane. Therefore, the block-co-polymer membranes require higher humidities to achieve sufficient conductivities than the Nafion membranes. An increase of RH above 87 % might over-proportionally boost the performance of the block-co-polymer membranes.

A series of block-co-polymer membranes with different IECs were tested in a H_2/air fuel cell with Nafion-based electrodes (see Fig. 10 and SI-8). As a membrane's conductivity and performance correlate to its detected high-frequency resistance (HFR) in the fuel cell test, Table 3 summarizes the thicknesses and the averaged HFRs of the tested membranes and compares them to literature data of Nafion membranes.

The HFR of the block-co-polymer decreases with its IEC down to 49 mOhm cm^2 , which resembles the trends from the ex-situ conductivity measurements. Consequently, the conductivity of the tetrablock membrane with the highest IEC clearly outperforms the commercial Nafion membrane XL, while being in a similar range to the reported data of Nafion 211 and the thicker Nafion 212. All polarization curves show an open-circuit voltage of around 0.8 V, probably related to the unoptimized manufacturing of the membrane electrode assembly (MEA). As Nafion-electrodes were applied, an additional interface exists between the electrode and membrane ionomer. Nevertheless, the MEA with the high IEC membrane achieved a maximum power density of around 0.7 W cm^{-2} . Besides proving the general applicability of the block-co-polymers in fuel cell experiments, this result already challenges optimized MEAs from established hydrocarbon materials, summarized in the literature [59].

The block-co-polymer membrane T1-90 consistently outperforms the established Nafion XL in the conductivity tests at high RH, and a related membrane shows auspicious fuel cell performance. Focusing the fluorine atoms within the polymer onto the aromatic groups increases the acidity of the ion-exchange groups and avoids fluorinated alkyl chains. As up to 40 % of the thiol groups in the membranes are involved in self-cross-linking, the number of ion-exchange groups is reduced (see section 3.4.2). Shifting this ratio to a higher amount of sulfonic acid groups might further enhance the conductivities of respective membranes. Besides alternative nonpolar polymer blocks, our lab will further investigate partial pre-oxidation of the thiol groups to balance membrane stability and conductivity.

4. Conclusion

sPPFS promises high proton conductivities in PEM applications but ultimately suffers from high brittleness and uncontrollable formation of cross-links. By synthesizing block-co-polymers based on sPPFS and POS, we improved the flexibility while establishing proton-conductive nanochannels. Moreover, the block-co-polymers only include aromatic fluorine atoms to increase the functional group's acidity and avoid PFAS-containing substances. Mesophase simulations of the block-co-polymers predicted bi-continuous nanostructures, which were verified by STEM imaging. Keeping the precursor polymer in a dispersion delayed cross-link formation until completed membrane fabrication. During the drying, membrane self-reinforcement occurred by thiol cross-links, which limited the water uptake and prevented membrane dissolution. Delaying solvent evaporation from the casted thin film reduces the membrane's stiffness, implying the impact of manufacturing on the cross-linking. The presented membranes were able to compete and even outperform the proton conductivity of commercial Nafion XL at high humidities. These unique properties make the presented block-co-polymers a promising candidate for future PFAS-free fuel cell and electrolyzer applications.

CRedit authorship contribution statement

Sebastian Auffarth: Writing – original draft, Visualization, Methodology, Investigation, Data curation, Conceptualization. **Maximilian Maier:** Writing – review & editing, Investigation. **Philipp Martschin:** Writing – review & editing, Visualization. **Theresa Stigler:** Writing – review & editing, Investigation. **Maximilian Wagner:** Writing – review & editing, Software. **Thomas Böhm:** Writing – review & editing, Investigation. **Andreas Hutzler:** Writing – review & editing, Visualization, Investigation, Data curation. **Simon Thiele:** Writing – review & editing, Supervision, Funding acquisition. **Jochen Kerres:** Writing –

review & editing, Supervision.

Declaration of competing interest

The authors declare that they have no known competing financial interests or personal relationships that could have appeared to influence the work reported in this paper.

Data availability

Data will be made available on request.

Acknowledgments

The authors acknowledge financial support from the Bavarian Ministry of Economic Affairs, Regional Development and Energy (project number: 44-6665a2/132/1) and the German Federal Ministry of Education and Research BMBF (03SF0771).

Appendix A. Supplementary data

Supplementary data to this article can be found online at <https://doi.org/10.1016/j.mtadv.2024.100521>.

References

- [1] H. Brunn, G. Arnold, W. Körner, G. Rippen, K.G. Steinhäuser, I. Valentin, PFAS: forever chemicals—persistent, bioaccumulative and mobile. Reviewing the status and the need for their phase out and remediation of contaminated sites, *Environ. Sci. Eur.* 35 (2023) 1–50, <https://doi.org/10.1186/s12302-023-00721-8>.
- [2] Z. Wang, A.M. Buser, I.T. Cousins, S. Demattio, W. Drost, O. Johansson, K. Ohno, G. Patlewicz, A.M. Richard, G.W. Walker, G.S. White, E. Leinala, A new OECD definition for per- and polyfluoroalkyl substances, *Environ. Sci. Technol.* 55 (2021) 15575–15578, <https://doi.org/10.1021/acs.est.1c06896>.
- [3] J. Zhou, K. Baumann, J.D. Surratt, B.J. Turpin, Legacy and emerging airborne per- and polyfluoroalkyl substances (PFAS) collected on PM_{2.5} filters in close proximity to a fluoropolymer manufacturing facility, *Environ. Sci. Process. Impacts* 24 (2022) 2272–2283, <https://doi.org/10.1039/d2em00358a>.
- [4] Z. Abunada, M.Y.D. Alazaiza, M.J.K. Bashir, An overview of per- and polyfluoroalkyl substances (PFAS) in the environment: source, fate, risk and regulations, *Water* 12 (2020) 3590, <https://doi.org/10.3390/w12123590>.
- [5] M. Houde, J.W. Martin, R.J. Letcher, K.R. Solomon, D.C.G. Muir, Biological monitoring of polyfluoroalkyl substances: a review, *Environ. Sci. Technol.* 40 (2006) 3463–3473, <https://doi.org/10.1021/es052580b>.
- [6] European Environment Agency, *Emerging Chemical Risks in Europe 'PFAS'*, Publications Office, 2019.
- [7] X. Lim, Could the world go PFAS-free? Proposal to ban 'forever chemicals' fuels debate, *Nature* 620 (2023) 24–27, <https://doi.org/10.1038/d41586-023-02444-5>.
- [8] S.S. White, J.P. Stanko, K. Kato, A.M. Calafat, E.P. Hines, S.E. Fenton, Gestational and chronic low-dose PFOA exposures and mammary gland growth and differentiation in three generations of CD-1 mice, *Environ. Health Perspect.* 119 (2011) 1070–1076, <https://doi.org/10.1289/ehp.1002741>.
- [9] S.E. Fenton, J.L. Reiner, S.F. Nakayama, A.D. Delinsky, J.P. Stanko, E.P. Hines, S. S. White, A.B. Lindstrom, M.J. Strynar, S.-S.E. Petropoulou, Analysis of PFOA in dosed CD-1 mice. Part 2. Disposition of PFOA in tissues and fluids from pregnant and lactating mice and their pups, *Reprod. Toxicol.* 27 (2009) 365–372, <https://doi.org/10.1016/j.reprotox.2009.02.012>.
- [10] V. Barry, A. Winquist, K. Steenland, Perfluorooctanoic acid (PFOA) exposures and incident cancers among adults living near a chemical plant, *Environ. Health Perspect.* 121 (2013) 1313–1318, <https://doi.org/10.1289/ehp.1306615>.
- [11] M. Carmo, D.L. Fritz, J. Mergel, D. Stolten, A comprehensive review on PEM water electrolysis, *Int. J. Hydrogen Energy* 38 (2013) 4901–4934, <https://doi.org/10.1016/j.ijhydene.2013.01.151>.
- [12] Y. Wang, D.F. Ruiz Diaz, K.S. Chen, Z. Wang, X.C. Adroher, Materials, technological status, and fundamentals of PEM fuel cells – a review, *Mater. Today* 32 (2020) 178–203, <https://doi.org/10.1016/j.mattod.2019.06.005>.
- [13] S. Auffarth, W. Daffinger, J. Mehler, V. Ardizzon, P. Preuster, P. Wasserscheid, S. Thiele, J. Kerres, Cross-linked proton-exchange membranes with strongly reduced fuel crossover and increased chemical stability for direct-isopropanol fuel cells, *J. Mater. Chem. A* 10 (2022) 17208–17216, <https://doi.org/10.1039/D2TA03832C>.
- [14] A. Kusoglu, A.Z. Weber, New insights into perfluorinated sulfonic-acid ionomers, *Chem. Rev.* 117 (2017) 987–1104, <https://doi.org/10.1021/acs.chemrev.6b00159>.
- [15] F.I. Allen, L.R. Comolli, A. Kusoglu, M.A. Modestino, A.M. Minor, A.Z. Weber, Morphology of hydrated as-cast nafion revealed through cryo electron tomography, *ACS Macro Lett.* 4 (2015) 1–5, <https://doi.org/10.1021/mz500606h>.
- [16] M. Feng, R. Qu, Z. Wei, L. Wang, P. Sun, Z. Wang, Characterization of the thermolysis products of Nafion membrane: a potential source of perfluorinated compounds in the environment, *Sci. Rep.* 5 (2015) 9859, <https://doi.org/10.1038/srep09859>.
- [17] M. Bonanno, K. Müller, B. Bensmann, R. Hanke-Rauschenbach, D. Aili, T. Franken, A. Chromik, R. Peach, A.T.S. Freiberg, S. Thiele, Review and prospects of PEM water electrolysis at elevated temperature operation, *Adv Materials Technologies* 9 (2024) 2300281, <https://doi.org/10.1002/admt.202300281>.
- [18] S. Ryu, B. Lee, J.-H. Kim, C. Pak, S.-H. Moon, High-temperature operation of PEMFC using pore-filling PTFE/Nafion composite membrane treated with electric field, *Int. J. Energy Res.* 45 (2021) 19136–19146, <https://doi.org/10.1002/er.7017>.
- [19] J.-D. Kim, A. Ohira, Water electrolysis using a porous IrO₂/Ti/IrO₂ catalyst electrode and nafion membranes at elevated temperatures, *Membranes* 11 (2021) 330, <https://doi.org/10.3390/membranes11050330>.
- [20] T. Stigler, M. Wagner, S. Thiele, J. Kerres, Modification of phosphonated poly(pentafluorostyrene) toward ductile membranes for electrochemical applications, *Macromolecules* 57 (2024) 364–372, <https://doi.org/10.1021/acs.macromol.3c01193>.
- [21] W. Gui, H. Guo, X. Chen, J. Wang, Y. Guo, H. Zhang, X. Zhou, Y. Zhao, J. Dai, Emerging polyfluorinated compound Nafion by-product 2 disturbs intestinal homeostasis in zebrafish (*Danio rerio*), *Ecotoxicol. Environ. Saf.* 249 (2023) 114368, <https://doi.org/10.1016/j.ecoenv.2022.114368>.
- [22] Z. Wang, J. Yao, H. Guo, N. Sheng, Y. Guo, J. Dai, Comparative hepatotoxicity of a novel perfluoroalkyl ether sulfonic acid, nafion byproduct 2 (H-PFMOZOSA), and legacy perfluorooctane sulfonate (PFOS) in adult male mice, *Environ. Sci. Technol.* 56 (2022) 10183–10192, <https://doi.org/10.1021/acs.est.2c00957>.
- [23] Y.A. Elabd, M.A. Hickner, Block copolymers for fuel cells, *Macromolecules* 44 (2011) 1–11, <https://doi.org/10.1021/ma101247c>.
- [24] T. Huang, J.M. Messman, K. Hong, J.W. Mays, Novel amphiphilic block copolymers derived from the selective fluorination and sulfonation of poly(styrene- block -1,3-cyclohexadiene), *J. Polym. Sci. Polym. Chem.* 50 (2012) 338–345, <https://doi.org/10.1002/pola.25037>.
- [25] F. Schönberger, J. Kerres, Novel multiblock-co-ionomers as potential polymer electrolyte membrane materials, *J. Polym. Sci. Polym. Chem.* 45 (2007) 5237–5255, <https://doi.org/10.1002/pola.22269>.
- [26] A. Dyck, D. Fritsch, S.P. Nunes, Proton-conductive membranes of sulfonated polyphenylsulfone, *J. of Applied Polymer Sci* 86 (2002) 2820–2827, <https://doi.org/10.1002/app.11264>.
- [27] P.A. García-Salaberri, Proton exchange membranes for polymer electrolyte fuel cells: an analysis of perfluorosulfonic acid and aromatic hydrocarbon ionomers, *Sustainable Materials and Technologies* 38 (2023) e00727, <https://doi.org/10.1016/j.susmat.2023.e00727>.
- [28] P. Xing, G.P. Robertson, M.D. Guiver, S.D. Mikhailenko, K. Wang, S. Kaliaguine, Synthesis and characterization of sulfonated poly(ether ether ketone) for proton exchange membranes, *J. Membr. Sci.* 229 (2004) 95–106, <https://doi.org/10.1016/j.memsci.2003.09.019>.
- [29] N. Ureña, M.T. Pérez-Prior, B. Levenfeld, P.A. García-Salaberri, On the conductivity of proton-exchange membranes based on multiblock copolymers of sulfonated polysulfone and polyphenylsulfone: an experimental and modeling study, *Polymers* 13 (2021), <https://doi.org/10.3390/polym13030363>.
- [30] S.M. Hossain, P. Patnaik, S. Sarkar, R. Sharma, U. Chatterjee, Ce–Mn bimetallic oxide-doped SPEEK/SPPPO blend composite membranes to induce high oxidative tolerance and proton conductivity for hydrogen fuel cells, *J. Mater. Chem. A* 12 (2024) 12628–12644, <https://doi.org/10.1039/D4TA00470A>.
- [31] M.J. Park, N.P. Balsara, Phase behavior of symmetric sulfonated block copolymers, *Macromolecules* 41 (2008) 3678–3687, <https://doi.org/10.1021/ma702733f>.
- [32] S.-Y. Jang, S.-H. Han, Characterization of sulfonated polystyrene-block-poly(ethyl-ran-propylene)-block-polystyrene copolymer for proton exchange membranes (PEMs), *J. Membr. Sci.* 444 (2013) 1–8, <https://doi.org/10.1016/j.memsci.2013.04.055>.
- [33] Y.A. Elabd, E. Napadensky, C.W. Walker, K.I. Winey, Transport properties of sulfonated poly(styrene-*b*-isobutylene-*b*-styrene) triblock copolymers at high ion-exchange capacities, *Macromolecules* 39 (2006) 399–407, <https://doi.org/10.1021/ma051958n>.
- [34] H. Nesterstedt, P. Jannasch, Poly(*p*-terphenyl alkylene)s grafted with highly acidic sulfonated polypentafluorostyrene side chains for proton exchange membranes, *J. Membr. Sci.* 647 (2022) 120270, <https://doi.org/10.1016/j.memsci.2022.120270>.
- [35] V. Atanasov, M. Bürger, S. Lyonard, L. Porcar, J. Kerres, Sulfonated poly(pentafluorostyrene): synthesis & characterization, *Solid State Ionics* 252 (2013) 75–83, <https://doi.org/10.1016/j.ssi.2013.06.010>.
- [36] M. Schuster, C.C. de Araujo, V. Atanasov, H.T. Andersen, K.-D. Kreuer, J. Maier, Highly sulfonated poly(phenylene sulfone): preparation and stability issues, *Macromolecules* 42 (2009) 3129–3137, <https://doi.org/10.1021/ma900333n>.
- [37] Stéphane Caron, Emma McInturf, Nucleophilic aromatic substitution, in: *Practical Synthetic Organic Chemistry*, John Wiley & Sons, Ltd, 2020, pp. 231–246.
- [38] C.D. Murphy, B.R. Clark, J. Amadio, Metabolism of fluoroorganic compounds in microorganisms: impacts for the environment and the production of fine chemicals, *Appl. Microbiol. Biotechnol.* 84 (2009) 617–629, <https://doi.org/10.1007/s00253-009-2127-0>.
- [39] S. Takamuku, A. Wohlfarth, A. Manhart, P. Räder, P. Jannasch, Hypersulfonated polyelectrolytes: preparation, stability and conductivity, *Polym. Chem.* 6 (2015) 1267–1274, <https://doi.org/10.1039/C4PY01177E>.
- [40] C. Langner, J. Meier-Haack, B. Voit, H. Komber, The stepped reaction of decafluorobiphenyl with thiophenol studied by in situ ¹⁹F NMR spectroscopy,

- J. Fluor. Chem. 156 (2013) 314–321, <https://doi.org/10.1016/j.jfluchem.2013.07.013>.
- [41] K. Ninomiya, N. Shida, T. Nishikawa, T. Ishihara, H. Nishiyama, I. Tomita, S. Inagi, Postfunctionalization of a perfluoroarene-containing π -conjugated polymer via nucleophilic aromatic substitution reaction, *ACS Macro Lett.* 9 (2020) 284–289, <https://doi.org/10.1021/acsmacrolett.9b01020>.
- [42] V. Atanasov, J. Kerres, ETFE-g-pentafluorostyrene: functionalization and proton conductivity, *Eur. Polym. J.* 63 (2015) 168–176, <https://doi.org/10.1016/j.eurpolymj.2014.12.017>.
- [43] S. Auffarth, M. Wagner, A. Krieger, B. Fritsch, L. Hager, A. Hutzler, T. Böhm, S. Thiele, J. Kerres, Nanophase-separated block-co-polymers based on phosphonated pentafluorostyrene and octylstyrene for proton-exchange membranes, *ACS Materials Lett.* (2023) 2039–2046, <https://doi.org/10.1021/acsmaterialslett.3c00569>.
- [44] K. Bosson, P. Marcasuzaa, A. Bousquet, G.E. Tovar, V. Atanasov, L. Billon, para fluoro-thiol clicked diblock-copolymer self-assembly: Towards a new paradigm for highly proton-conductive membranes, *J. Membr. Sci.* 659 (2022) 120796, <https://doi.org/10.1016/j.memsci.2022.120796>.
- [45] Z. Liu, N. MacRitchie, S. Pyne, N.J. Pyne, R. Bittman, Synthesis of (S)-FTY720 vinylphosphonate analogues and evaluation of their potential as sphingosine kinase 1 inhibitors and activators, *Bioorg. Med. Chem.* 21 (2013) 2503–2510, <https://doi.org/10.1016/j.bmc.2013.02.042>.
- [46] H.-A. Klok, S. Lecommandoux, Supramolecular materials via block copolymer self-assembly, *Adv. Mater.* 13 (2001) 1217, [https://doi.org/10.1002/1521-4095\(200108\)13:16<1217:AID-ADMA1217>3.0.CO;2-D](https://doi.org/10.1002/1521-4095(200108)13:16<1217:AID-ADMA1217>3.0.CO;2-D).
- [47] L. Leibler, Theory of microphase separation in block copolymers, *Macromolecules* 13 (1980) 1602–1617, <https://doi.org/10.1021/ma60078a047>.
- [48] J. Kamada, K. Koynov, C. Corten, A. Juhari, J.A. Yoon, M.W. Urban, A.C. Balazs, K. Matyjaszewski, Redox responsive behavior of thiol/disulfide-functionalized star polymers synthesized via atom transfer radical polymerization, *Macromolecules* 43 (2010) 4133–4139, <https://doi.org/10.1021/ma100365n>.
- [49] G. Socrates, *Infrared and Raman Characteristic Group Frequencies: Tables and Charts*, third. ed., Wiley, Chichester, 2010 repr. as paperback.
- [50] B. Fritsch, M. Wu, A. Hutzler, D. Zhou, R. Spruit, L. Vogl, J. Will, H. Hugo Pérez Garza, M. März, M.P.M. Jank, E. Spiecker, Sub-Kelvin thermometry for evaluating the local temperature stability within in situ TEM gas cells, *Ultramicroscopy* 235 (2022) 113494, <https://doi.org/10.1016/j.ultramic.2022.113494>.
- [51] E.M.W. Tsang, Z. Zhang, Z. Shi, T. Soboleva, S. Holdcroft, Considerations of macromolecular structure in the design of proton conducting polymer membranes: graft versus diblock polyelectrolytes, *J. Am. Chem. Soc.* 129 (2007) 15106–15107, <https://doi.org/10.1021/ja074765j>.
- [52] Q. Yuan, T. Zhou, L. Li, J. Zhang, X. Liu, X. Ke, A. Zhang, Hydrogen bond breaking of TPU upon heating: understanding from the viewpoints of molecular movements and enthalpy, *RSC Adv.* 5 (2015) 31153–31165, <https://doi.org/10.1039/C5RA03984C>.
- [53] Y. Tang, A.M. Karlsson, M.H. Santare, M. Gilbert, S. Cleghorn, W.B. Johnson, An experimental investigation of humidity and temperature effects on the mechanical properties of perfluorosulfonic acid membrane, *Materials Science and Engineering: A* 425 (2006) 297–304, <https://doi.org/10.1016/j.msea.2006.03.055>.
- [54] J. Kerres, A. Ullrich, M. Hein, V. Gogel, K.A. Friedrich, L. Jörissen, Cross-linked polyaryl blend membranes for polymer electrolyte fuel cells, *Fuel Cell.* 4 (2004) 105–112, <https://doi.org/10.1002/fuce.200400013>.
- [55] Z. Shang, M.M. Hossain, R. Wycisk, P.N. Pintauro, Poly(phenylene sulfonic acid)-expanded polytetrafluoroethylene composite membrane for low relative humidity operation in hydrogen fuel cells, *J. Power Sources* 535 (2022) 231375, <https://doi.org/10.1016/j.jpowsour.2022.231375>.
- [56] J. Peron, A. Mani, X. Zhao, D. Edwards, M. Adachi, T. Soboleva, Z. Shi, Z. Xie, T. Navessin, S. Holdcroft, Properties of Nafion® NR-211 membranes for PEMFCs, *J. Membr. Sci.* 356 (2010) 44–51, <https://doi.org/10.1016/j.memsci.2010.03.025>.
- [57] J. Yan, X. Huang, H.D. Moore, C.-Y. Wang, M.A. Hickner, Transport properties and fuel cell performance of sulfonated poly(imide) proton exchange membranes, *Int. J. Hydrogen Energy* 37 (2012) 6153–6160, <https://doi.org/10.1016/j.ijhydene.2011.09.092>.
- [58] H.-B. Song, J.-H. Park, J.-S. Park, M.-S. Kang, Pore-filled proton-exchange membranes with fluorinated moiety for fuel cell application, *Energies* 14 (2021) 4433, <https://doi.org/10.3390/en14154433>.
- [59] H. Nguyen, C. Klose, L. Metzler, S. Vierrath, M. Breitwieser, Fully hydrocarbon membrane electrode assemblies for proton exchange membrane fuel cells and electrolyzers: an engineering perspective, *Adv. Energy Mater.* 12 (2022) 2103559, <https://doi.org/10.1002/aenm.202103559>.